

Improving Velocity Gradient Technique with Principal Component Analysis

Yue Hu^{1,2}, Ka Ho Yuen²,[★] A. Lazarian²

¹College of Electronics and Information Engineering, Tongji University, Shanghai, China

²Department of Astronomy, University of Wisconsin-Madison, Madison, USA

Accepted XXX. Received YYY; in original form ZZZ

ABSTRACT

Probing magnetic field directions in interstellar medium is generally difficult even with the use of the polarimetry. Recent development of the Velocity Gradient Technique (VGT, [González-Casanova & Lazarian 2017](#); [Yuen & Lazarian 2017a](#)) allows observers to probe magnetic field directions with spectroscopic data. However, the quality of the spectroscopic maps highly influences the prediction of magnetic field directions using VGT. In this paper, we employ the method of Principle Component Analysis (PCA) to extract the turbulent part of the spectroscopic cubes for VGT to apply. By using synthetic observation data from numerical simulations, we show that PCA is similar to a method of wavenumber filtering along the velocity axis. With the filtering the performance of PCA-VGT is significantly improved in tracing magnetic field directions, especially in the presence of noise both in subsonic and supersonic region. We select a GALFA-HI region nearly Galactic zenith for testing.

Key words: ISM: structure — ISM: turbulence—magnetohydrodynamics (MHD) — methods: numerical

1 INTRODUCTION

Turbulence is ubiquitous across the universe in different scales ([Armstrong et al. 1995](#); [Chepurnov & Lazarian 2010](#)) and magnetic field plays an important role in interacting and regulating with the fluid motions, especially in the case of interstellar medium (ISM) which is both turbulent and magnetized ([McKee & Ostriker 2007](#); [Chepurnov & Lazarian 2009](#)). However, the study of magnetic fields in the ISM is complicated and often inaccurate. For instance, with the best satellite equipment like BlastPol or Planck, the polarization percentage from dust grain alignment ([Hall 1949](#); [Hiltner 1949](#), See [Andersson et al. 2015](#) for a review) is drastically low especially near the galactic plane, precluding the observers to draw any conclusion on the magnetic field morphology in the region with most interesting physical behavior.

The understanding of the role of magnetized turbulence is not fully revealed until the recent theoretical breakthrough on MHD turbulence theory ([Goldreich & Sridhar 1995](#), hereafter GS95) supported by a number of theoretical ([Lazarian & Vishniac 1999](#)) and numerical works ([Cho et al. 2002](#); [Cho & Lazarian 2003](#); [Kowal et al. 2009](#)). With the new picture of MHD turbulence, the proposal of using spectroscopic veloc-

ity gradients to trace magnetic field, Velocity Gradient Technique (VGT, [González-Casanova & Lazarian 2017](#); [Yuen & Lazarian 2017a,b](#); [Lazarian & Yuen 2018a](#)), is recently proposed and widely applied to observation data from HI to self-gravitating molecular clouds. The orientations of velocity gradients are taken into account for tracing both the direction of magnetic field in diffuse ([Yuen & Lazarian 2017a](#)) and self-gravitating media ([Yuen & Lazarian 2017b](#); [Lazarian & Yuen 2018a](#)), and also estimations of the sonic (M_s , [Yuen et al. 2018a](#)) and Alfvénic (M_A , [Lazarian et al. 2018](#)) Mach numbers in the framework of gradients. The vast applications of VGT illustrate its capability to trace magnetic fields in different regimes.

The application of VGT relies on high quality data. Observational data usually contains noises from instruments and other astronomical objects. Even with high enough signal-to-noise (S/N) ratio, the spatial structure which VGT highly relies on would nevertheless be distorted. Noise suppression method for VGT perpendicular to the line of sight has been explored in [Lazarian et al. \(2017\)](#) and thoughtfully restudied in [Lazarian & Yuen \(2018a\)](#), showing that a convolution of the observation map with a small σ Gaussian kernel would retrieve the spatial structure of the molecular cloud. Moreover, in [Yuen & Lazarian \(2017b\)](#) they showed that the filtering of non-turbulence contribution in Fourier space can improve the accuracy of VGT in tracing magnetic

[★] E-mail: kyuen2@wisc.edu

Model Name	M_S	M_A	Resolution
Ms0.4Ma0.04	0.41	0.04	480 ³
Ms0.8Ma0.08	0.92	0.09	480 ³
Ms1.6Ma0.16	1.95	0.18	480 ³
Ms3.2Ma0.32	3.88	0.35	480 ³
Ms6.4Ma0.64	7.14	0.66	480 ³

Table 1. Descriptions of the MHD simulation cubes used in the present work. M_S and M_A are the instantaneous values at each the snapshots are taken.

field. However, there does not have a way to filter noises from signals along the velocity axis. In terms of position-position-velocity (PPV) data we currently do not have a way to filter contributions from specific wavenumbers along the velocity axis, not to mention filtering the non-turbulence part along it. Therefore the application of VGT is limited to noise or non-turbulence dominated PPV cubes when tracing magnetic field directions.

The method of Principle Component Analysis (PCA) is widely used in image processing and image compression. The idea behind PCA lies on the fact that an image of size N^2 can be effectively represented by $n < N$ eigen-maps. In the context of turbulence studies, Brunt & Heyer (2002a,b) investigated how PCA may find the turbulence spectral index in an empirical framework. They found that by applying PCA on the covariance matrix of the PPV spectroscopic cubes, it is possible to use the eigen-images from the largest eigenvalues to study turbulence scaling. The physical meaning of the eigenvalues from the PCA analysis are closely related to the size of turbulence velocity v^2 . In particular, those larger eigenvalues corresponds to the largest scale contributions of turbulence eddies along the line of sight $v^2 \sim (l^{1/3})^2 \sim l^{2/3}$, assuming GS95 scaling applies. Later Heyer et al. (2008) applied and improved this method to study turbulence anisotropy of Taurus¹. In the perspective of VGT, the individual eigen-image found in Brunt & Heyer (2002b) are eligible for studying magnetic field directions due to the contribution of turbulent eddies with different size.

In what follows, we briefly describe the numerical code and setup for simulation in §2. In §3, we test the implementation of PCA with VGT in numerical simulations. §4 shows the observational example with PCA-VGT. In §5, we give our discussion about our technique and conclusion.

2 NUMERICAL SETTING FOR SYNERGISTIC USE OF PCA AND VGT

For our studies of gradients with PCA, we reuse the numerical cubes in Lazarian & Yuen (2018a). The simulation parameters with different combinations of Alfvénic Mach numbers M_A and sonic Mach numbers M_S are listed in Table 1.

In order to simplify the complexity of employing PCA to VGT, we therefore only consider the optically thin case ($\tau \sim \int \kappa(s)ds \ll 1$) and synthesize observational maps similar

to that in Yuen et al. (2018b) : We denote the pixel values of the PPV cubes as $\rho(x, y, v)$, and the cubes dimensions $n_x \times n_y \times n_v$, where the n_v means the number of velocity channels along the spectral line direction v (line-of-sight direction, LOS), which is $n_v = 400$ for our studies unless specifically mentioned.

The PPV cubes will be preprocessed first by the treatment of PCA similar to the pipeline in Brunt & Heyer (2002b), and then be passed to VGT for the magnetic field studies for different eddy scales. The product of PCA would be a set of eigen-images I_i with decreasing order of eigen-values $\lambda_i \sim v_i^2$, where the latter records the velocity variance along the line of sight. As we discussed in the §1 that the velocity variance is related to the eddy size along the line of sight provided that the respective scale is turbulence-dominated, we shall investigate which eigen-images would allow us to retrieve the contribution of turbulence motions in the PPV cube.

Assumed properly normalized², we can treat the PPV cube $\rho(x, y, v)$ as the probability density function of three random variables x, y, v , we can then define the covariance matrix (Brunt & Heyer 2002a)³

$$S(v_1, v_2) \propto \int dx dy \rho(x, y, v_1) \rho(x, y, v_2) \quad (1)$$

One can solve a eigenvalue equation for this covariance matrix:

$$S\mathbf{u} = \lambda\mathbf{u} \quad (2)$$

where the λ_i are the eigenvalues associated with the eigenvectors \mathbf{u}_i with $i = 1, 2, \dots, n_v$. The eigenvectors \mathbf{u}_i contain the weight of how one can construct the eigen-maps of rank i with the channel maps. We apply eigenvalues λ_i as the weighting coefficients for each channel. Then the eigen-intensity maps $I_{si-eigen}$ and eigen-centroid maps $C_{si-eigen}$ can be computed by:

$$C_{si-eigen}(x, y) = \frac{\int dv \rho(x, y, v) \cdot v \cdot \lambda(v)}{I_{si-eigen}(x, y)} \quad (3)$$

$$I_{si-eigen}(x, y) = \int dv \rho(x, y, v) \cdot \lambda(v) \quad (4)$$

For the gradient computation we shall follow the sub-block averaging method developed in Yuen & Lazarian (2017a), which will tell the *sub-block averaged orientation* of gradients. The resultant gradients will be rotated 90° to predict the magnetic field directions. The error estimation method (Lazarian & Yuen 2018a) would also be employed to signify how accurate the Gaussian fitting function used in sub-block averaging is when computing the average gradient direction within a sub-block. The orientation of gradients from VGT is compared with the synthetic polarization assuming a constant emissivity in dust grain alignment

² In principle one shall use the normalized PPV cube $\rho' = \rho / \int \rho$. However for the treatment of PCA, the difference of a constant does not alter the result. Therefore we stay with ρ for simplicity.

³ The textbook definition of covariance matrix should be $S(v_1, v_2) = E(\rho(v_1)\rho(v_2)) - E(\rho(v_1))E(\rho(v_2))$, where E is the expectation operator. However both Brunt & Heyer (2002a,b) and Heyer et al. (2008) did not include the second part. In the time being, we shall assume the contribution of eigen-modes from the $E(\rho(v_1))E(\rho(v_2))$ part to be infinitesimal.

¹ In Yuen et al. (2018b) we showed that PCA itself cannot trace magnetic field accurately compared to both VGT and the method of Correlation Function Anisotropy (Esquivel & Lazarian 2005).

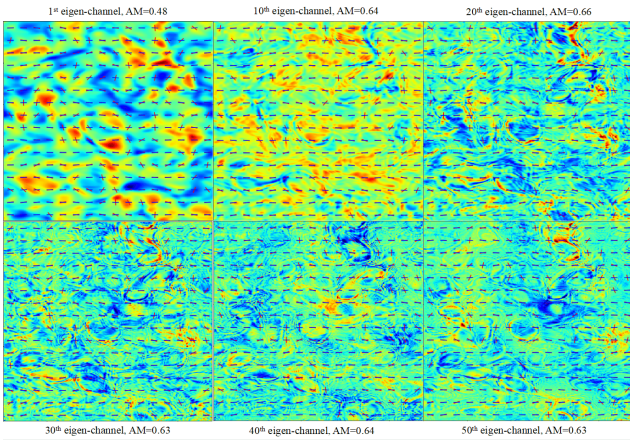


Figure 1. The eigen-centroid maps with gradients (red) and magnetic field (blue) plotted with different eigenvalues.

process (Lazarian 2007). That means the Stokes parameters $Q(x, y)$ and $U(x, y)$ can be expressed in terms of the angle θ between the x and y direction magnetic fields by $\tan \theta(x, y, z) = B_y(x, y, z)/B_x(x, y, z)$:

$$Q(x, y) \propto \int dz \rho(x, y, z) \cos(2\theta(x, y, z)) \quad (5)$$

$$U(x, y) \propto \int dz \rho(x, y, z) \sin(2\theta(x, y, z)) \quad (6)$$

The polarization angle $\Phi = 0.5 \arctan(U/Q)$ is then defined correspondingly, which gives an probe of projected magnetic field in realistic scenarios.

The relative orientations between the 90° rotated gradients and project magnetic field directions from polarization angles are measured by the **Alignment Measure (AM)** used in previous studies (González-Casanova & Lazarian 2017; Yuen & Lazarian 2017a): $AM = 2(\langle \cos^2 \theta_r \rangle - \frac{1}{2})$, where θ_r is the relative angle between the gradients (rotated 90°) and the direction of projected magnetic field. The range of AM is $[-1, 1]$. When $AM = 1$, the gradients (rotated 90°) are parallel to the projected magnetic field. When $AM = -1$, the gradients (rotated 90°) are perpendicular to the projected magnetic field. We expect to get $AM \sim 1$ in most scenarios.

3 APPLYING VGT TO EIGEN-IMAGES

We would first like to know how structurally the eigen-images from different eigenvalues would behave when comparing with magnetic field directions. We compute the sub-block averaged gradients for each eigen-images and compare with the projected magnetic field directions in Fig. 1 showing the gradients and the structure of some selected eigen-centroids for the cube $M_s 0.4 M_A 0.04$. One can see for the eigen-centroids with smaller eigenvalues (larger rank), the alignment measure tends to be come larger, and the structure of the eigen-centroids becomes more filamentary.

We analyze the visual patterns in Fig. 1 using the AM-eigenvalue plot. The pink curves in Fig. 2 shows how the AM of the gradients from eigen-images and projected magnetic field varies with respect to the eigenvalues from PCA analysis for the numerical cubes listed in Table 1. To test

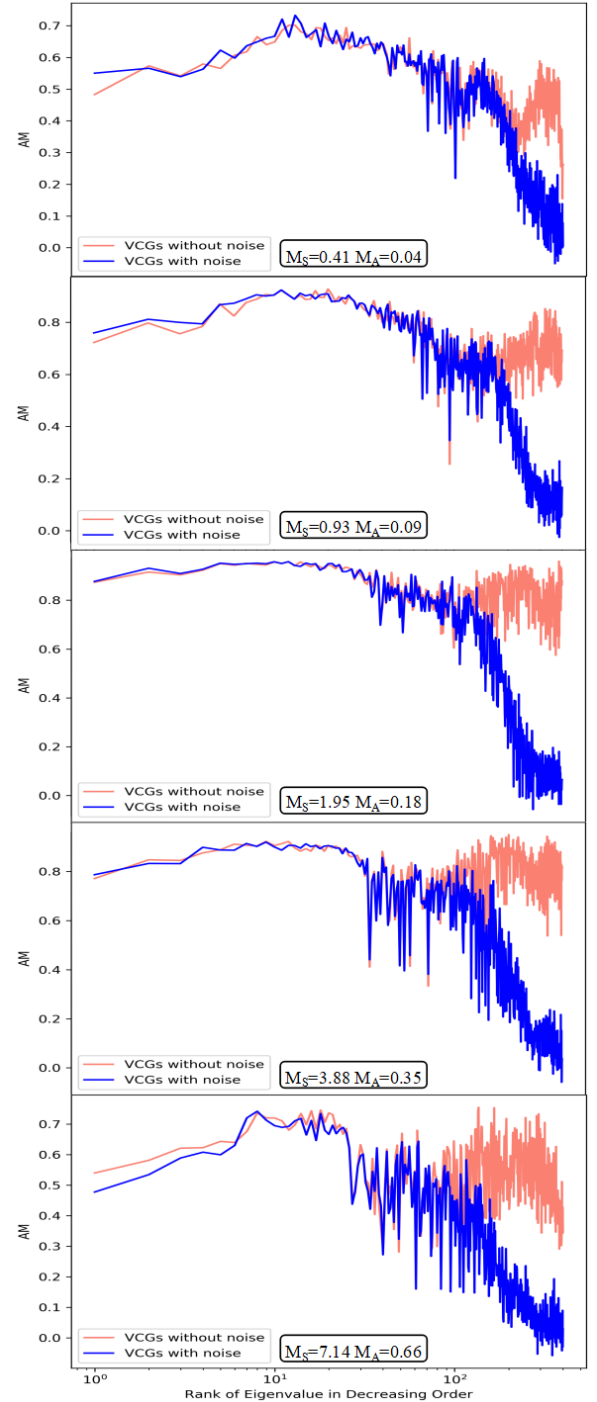


Figure 2. Five plots showing the response of AM between gradients of eigen-centroids and projected magnetic field to the rank of eigenvalue for both noiseless (pink) and noisy (blue) cases.

the power of PCA on noise removal, we add white noises with mean amplitude $0.1\sigma_C$ to the centroid maps, which are illustrated as the blue curves in Fig. 2. The x-axis in Fig. 2 represents the *rank of eigenvalues* sorted in decreasing order, i.e. if $\lambda_1 > \lambda_2 > \dots > \lambda_n$, then we shall use the number 1 (the rank) to represent λ_1 , rank 2 for λ_2 etc. We see that for all simulations we tested, the peak rank is at around ~ 10 . As the rank increases (i.e. smaller eigenvalues), the AM of

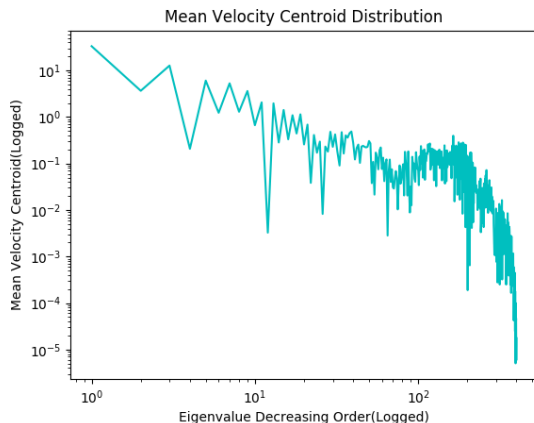


Figure 3. A plot showing how the eigen-centroid amplitudes varies with the rank of the eigen-values on the synthetic map from the cube Ms0.4Ma0.04.

the respective gradients of eigen-centroids to magnetic field decreases significantly. In noisy environments (blue curves in Fig. 2), the AM of the small ranks are approximately the same as the noiseless case (pink curves), but the AM in higher rank cases drop significantly. The experiment in Fig. 2 shows that using the method of PCA before applying VGT, we can retrieve the strong signal part, which has a lower rank in PCA, from the noisy part, which has a higher rank.

We also spot that the AM in rank $\sim 1 - 5$ is in generally smaller than that in rank $\sim 10 - 15$. The reason behind is because the largest v^2 extracted from PCA corresponds to the largest-scale eddies along the line of sight, which may not be fully turbulent compared to those with rank $\sim 10 - 15$. With the consideration that $v^2 \sim l^{2/3}$, the range of rank at $10 - 15$ should corresponds to the turbulent eddies in the inertial ranges of our numerical cubes ($k_{inertial} \approx 10 - 30$). In fact, when we refer to the eigen-centroid amplitudes from the cube Ms0.4Ma0.04 (Fig 3), we can see the amplitude becomes insignificant after rank > 20 . The amplitude of the eigen-centroids with rank higher than 20 is at least $0.1 - 0.01$ compared to the first few eigen-centroids. Therefore to use PCA with VGT in full potential, observers need to remove the largest eigenvalues together with those having rank > 20 to obtain the best result in tracing magnetic field with VGT.

4 APPLICATION TO OBSERVATION

For testing our recipe we use the well-studied region from Clark et al. (2015), in which the respective survey can further information can be found in Peek et al. (2018). The region spans right ascension (R.A.) 195° to 265° and declination (DEC) 19.1° to 38.3° , covering a very large piece of HI region with different physical conditions. The HI-cube has 41 velocity channels with each $\sim 3\text{ km/s}$ wide. In previous works (Yuen et al. 2018a; Lazarian et al. 2018) we studied M_s and M_A respectively in the same region, showing the region is super-sonic and sub-Alfvénic ($M_A \sim 0.75$), which is close to the condition we had in Table 1. We then would use the same strategy as we did in §3 to analyze the gradient orientation with PCA.

We apply PCA the selected region and choose the 2^{nd} and 10^{th} eigen-centroid maps based on the prediction we had in Fig 2. We illustrate the magnetic field tracing with VGT and compare it to the magnetic field directions traced by the 353GHz Planck polarization data, which we illustrated in Fig.4 with two eigen-centroid maps λ_2 and λ_{10} . The corresponding figure showing the AM-eigenvalue variation is in Fig 5, which has the same trend as Fig 2. The 10^{th} eigen-map has an obviously better AM compared to that of 2^{nd} , which is consistent to the study we have in §3.

5 DISCUSSION & CONCLUSION

It is expected that PCA can extract the most important contributions in the image by sorting the eigenvalues from PCA. In the present work we utilize the properties of the eigenvalues and eigenvectors of PCA and test whether the gradients of eigen-centroids can provide better estimation of magnetic field directions compared to traditional method in González-Casanova & Lazarian (2017) & Yuen & Lazarian (2017a). We show that both in synthetic and real observational maps, the extraction of eigen-centroids in the rank number of ~ 10 can effectively probe the direction of magnetic field with a very high AM. As a result, for the studies of projected magnetic field the PCA-VGT method we addressed in §3 can provide a very high accuracy tracing independent of polarimetry measurement.

The employment of eigen-value decompositions through PCA also provides a way to study three-dimensional (3D) magnetic field. As we can isolate the contribution of turbulent eddies along the line of sight with PCA, we can then stack the prediction from different eigen-centroids and construct the 3D tomography by sorting the eigenvalue axis. In a separate development the gradients of synchrotron intensity (Lazarian et al. 2017) and polarization intensity (Lazarian & Yuen 2018b) have been used to construct the 3D magnetic field morphology with multi-frequency measurements. Similar idea of constructing 3D magnetic field morphology with VGT on spectroscopic data has been tested in González-Casanova & Lazarian (2018) when the galactic rotation curve is available. With these 3D field tracing methods available, the rich application of VGT and synergy with different techniques will then shift the paradigm of studying magnetic fields from polarimetry measurements to studies of gradients on both interferometric and spectroscopic data.

ACKNOWLEDGEMENTS

AL acknowledges the support the NSF grant DMS 1622353 and AST 1715754. This publication utilizes data from Galactic ALFA HI (GALFA HI) survey data set obtained with the Arecibo L-band Feed Array (ALFA) on the Arecibo 305m telescope. The Arecibo Observatory is operated by SRI International under a cooperative agreement with the National Science Foundation (AST-1100968), and in alliance with Ana G. Méndez-Universidad Metropolitana, and the Universities Space Research Association. The GALFA HI surveys have been funded by the NSF through grants to Columbia University, the University of Wisconsin, and the University of California.

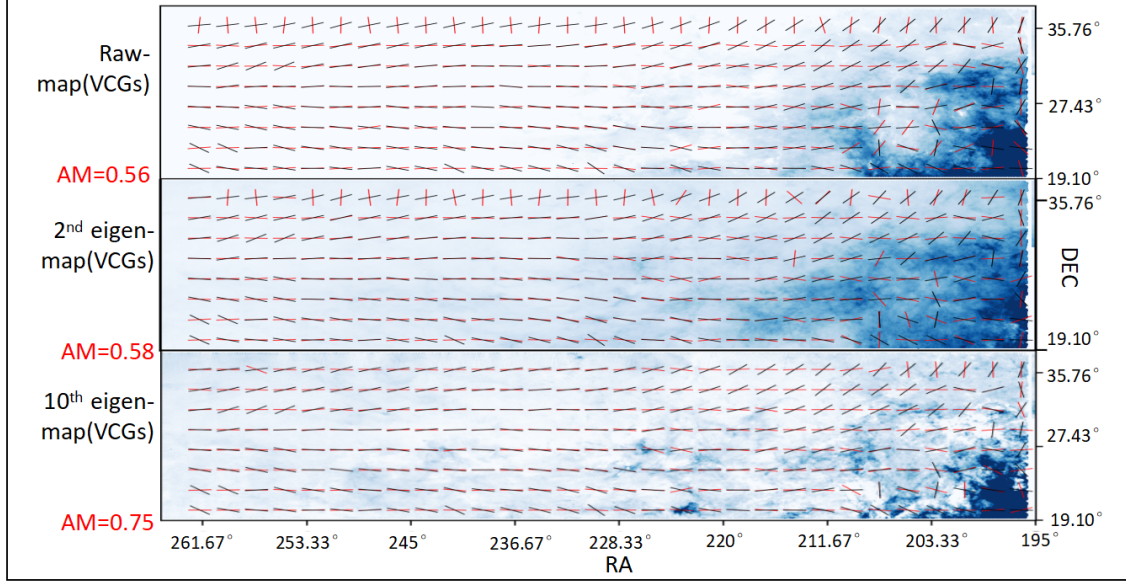


Figure 4. The region is from GALFA-HI and spans right ascension 195° to 265° and declination 19.1° to 38.3° , stretches from $b = 30^\circ$ above the Galactic plane to $b = 81.7^\circ$, nearly Galactic zenith. We compare the gradients got from VCGs (red lines) with the magnetic field obtained from Planck polarization data (black lines).

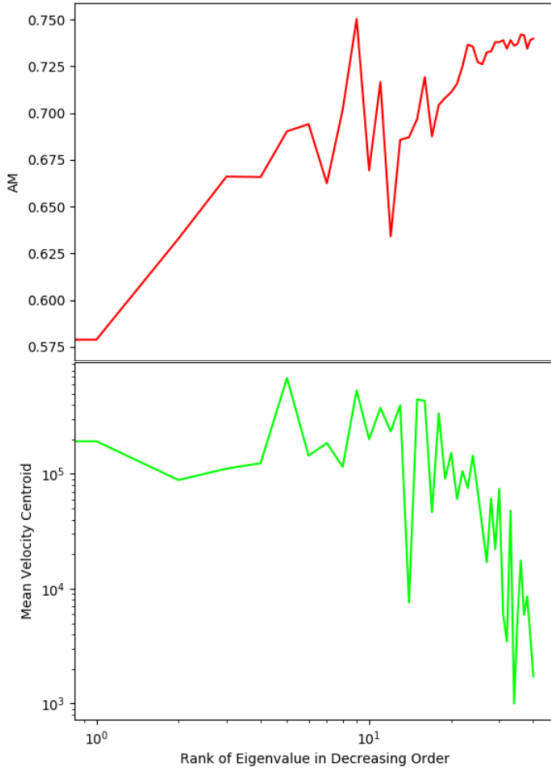


Figure 5. A plot showing the AM (top) and mean centroid amplitude (bottom) versus the rank of the eigen-values on the PPV cube from observation

REFERENCES

- Armstrong, J. W., Rickett, B. J., & Spangler, S. R. 1995, *ApJ*, 443, 209
 Andersson, B.-G., Lazarian, A., & Vaillancourt, J. E. 2015, *ARA&A*, 53, 501

- Brunt, C. M., & Heyer, M. H. 2002a, *ApJ*, 566, 276
 Brunt, C. M., & Heyer, M. H. 2002b, *ApJ*, 566, 289
 Chepurnov, A., & Lazarian, A. 2009, *ApJ*, 693, 1074
 Chepurnov, A., & Lazarian, A. 2010, *ApJ*, 710, 853
 Cho, J., Lazarian, A., & Vishniac, E. T. 2002, *ApJ*, 566, L49
 Cho, J., & Lazarian, A. 2003, *MNRAS*, 345, 325
 Clark, D. S., Marinak, M. M., Weber, C. R., et al. 2015, *Physics of Plasmas*, 22, 022703
 Esquivel, A., & Lazarian, A. 2005, *ApJ*, 631, 320
 Goldreich, P., & Sridhar, S. 1995, *ApJ*, 438, 763
 González-Casanova, D. F., & Lazarian, A. 2017, *ApJ*, 835, 41
 González-Casanova, D. F., & Lazarian, A. 2018, in prep
 Heyer, M., Gong, H., Ostriker, E., & Brunt, C. 2008, *ApJ*, 680, 420-427
 Hall, J. S. 1949, *Science*, 109, 166
 Hiltner, W. A. 1949, *Science*, 109, 165
 Kowal, G., Lazarian, A., Vishniac, E. T., & Otmianowska-Mazur, K. 2009, *ApJ*, 700, 63
 Lazarian, A. 2007, *J. Quant. Spectrosc. Radiative Transfer*, 106, 225
 Lazarian, A. 2016, *ApJ*, 833, 131
 Lazarian, A., & Vishniac, E. T. 1999, *ApJ*, 517, 700
 Lazarian, A., & Yuen, K. H. 2018, *ApJ*, 853, 96
 Lazarian, A., & Yuen, K. H. 2018, arXiv:1802.00028
 Lazarian, A., Pogossyan, D., & Esquivel, A. 2002, *Seeing Through the Dust: The Detection of HI and the Exploration of the ISM in Galaxies*, 276, 182
 Lazarian, A., Yuen, K. H., Lee, H., & Cho, J. 2017, *ApJ*, 842, 30
 Lazarian, A., Yuen, K. H., Ho, K. W., et al. 2018, arXiv:1802.02984
 McKee, C. F., & Ostriker, E. C. 2007, *ARA&A*, 45, 565
 Peek, J. E. G., Babler, B. L., Zheng, Y., et al. 2018, *ApJS*, 234, 2
 Yuen, K. H., & Lazarian, A. 2017, *ApJ*, 837, L24
 Yuen, K. H., & Lazarian, A. 2017, arXiv:1703.03026
 Yuen, K. H., & Lazarian, A. 2018, in prep.
 Yuen, K. H., Lazarian, V., & Lazarian, A. 2018, arXiv:1802.00024
 Yuen, K. H., Chen, J., Ho, K. W., et al. 2018, in prep